Acta Oceanol. Sin., 2022, Vol. 41, No. 2, P. 166–179
https://doi.org/10.1007/s13131-021-1704-7
http://www.aosocean.com
E-mail: ocean2@hyxb.org.cn

Signal quality analysis and quality check of BDS3 Precise Point Positioning in the Arctic Ocean

Xiaoguo Guan[1]*, Hongzhou Chai[2], Guorui Xiao[2], Zhenqiang Du[2], Wenlong Qi[2], Xueping Wang[3]

[1] College of Urban and Environmental Sciences, Xuchang University, Xuchang 461000, China

[2] Institute of Geospatial Information, Information Engineering University, Zhengzhou 450001, China

[3] Department of Civil Engineering, Henan Vocational College of Water Conservancy and Environment, Zhengzhou 450001, China

Received 25 June 2019; accepted 8 November 2019

© Chinese Society for Oceanography and Springer-Verlag GmbH Germany, part of Springer Nature 2022

Abstract

This study analyzes the signal quality and the accuracy of BeiDou 3rd generation Satellite Navigation System (BDS3) Precise Point Positioning (PPP) in the Arctic Ocean. Assessment of signal quality of BDS3 includes signal to noise ratio (SNR), multipath (MP), dilution of precision (DOP), and code-minus-carrier combination (CC). The results show that, 5 to 13 satellites are visible at any time in the Arctic Ocean area as of September 2018, which are sufficient for positioning. In the mid-latitude oceanic region and in the Arctic Ocean, the SNR is 25–52 dB Hz and the MP ranges from –2 m to 2 m. As the latitude increases, the DOP values show large variation, which may be related to the distribution of BDS satellites. The CC values of signals B1I and BIC range from –5 m to 5 m in the mid-latitude sea area and the Arctic Ocean, which means the effect of pseudorange noise is small. Moreover, as to obtain the external precise reference value for GNSS positioning in the Arctic Ocean region is difficult, it is hard to evaluate the accuracy of positioning results. An improved isotropy-based protection level method based on Receiver Autonomous Integrity Monitoring is proposed in the paper, which adopts median filter to smooth the gross errors to assess the precision and reliability of PPP in the Arctic Ocean. At first, the improved algorithm is verified with the data from the International GNSS Service Station Tixi. Then the accuracy of BDS3 PPP in the Arctic Ocean is calculated based on the improved algorithm. Which shows that the kinematic accuracy of PPP can reach the decimeter level in both the horizontal and vertical directions, and it meets the precision requirements of maritime navigation.

Key words: BDS3, Arctic Ocean, signal quality analysis, protection level, quality check, Precise Point Positioning, satellite navigation

Citation: Guan Xiaoguo, Chai Hongzhou, Xiao Guorui, Du Zhenqiang, Qi Wenlong, Wang Xueping. 2022. Signal quality analysis and quality check of BDS3 Precise Point Positioning in the Arctic Ocean. Acta Oceanologica Sinica, 41(2): 166–179, doi: 10.1007/s13131-021-1704-7

1 Introduction

The BeiDou Navigation Satellite System (BDS), which was independently constructed and developed by China, aims to provide positioning, navigation, and timing (PNT) services globally (CSNO, 2019). The construction of BDS follows a "first-test, post-regional, and final-global" three-step strategy. The third-phase of this satellite navigation system is called BeiDou-3 (BDS3) (Yang, 2010). As a high-precision absolute positioning method, Precise Point Positioning (PPP) has extended its applications due to its global coverage, and high accuracy (Zumberge et al., 1997; Luo et al., 2018). In view of the advantages and characteristics of PPP technology, as well as the construction and development of BDS, BDS3 PPP has become one of the hot research topics in the field of satellite navigation and positioning technology (Xu et al., 2013; Tu et al., 2018). Moreover, the signal quality of BDS3 as well as the accuracy and reliability of positioning are of great significance for the promotion and application of satellite navigation in marine environment (Liu et al., 2017).

Factors affecting the signal quality of BDS have been analyzed in many studies including signal carrier-to-noise density ratio (SNR) (Hauschild et al., 2012; Xiao et al., 2016; Lou et al., 2018; Yang et al., 2018), the precision of observations (Montenbruck et al., 2013; Yang et al., 2014; Zhao et al., 2015), multipath effects (MP) (Li et al., 2014; Wang et al., 2015; Wanninger and Beer, 2015; Cai et al., 2016; Xu et al., 2018) and dilution of precision (DOP) (Gumilar et al., 2018; Wang et al., 2019). Although these investigations dealt with different aspects of BDS performance, most researches were focused on the conventional land-based environment. There are few studies on the signal quality of BDS3 in high latitudes Arctic Ocean (Luo et al., 2015). This is due to the fact that it is difficult to acquire the BDS3 data in high latitudes Arctic Ocean. The experiments always require a lot of manpower, material and financial resources. In addition, the BDS3 data is relatively new. Studies on the data quality and the positioning performance of PPP in the Arctic region are of great significance. Because it not only can provide information for broaden-

Foundation item: The Science and Technology of Henan Province under contract No. 212102310029; the National Natural Science Founation Cultivation Project of Xuchang University under contract No. 2022GJPY007; the Educational Teaching Research and Practice Project of Xuchang University under contract No. XCU2021-YB-024.

*Corresponding author, E-mail: guanguo666@163.com

ing the application of BDS particularly for the marine and high latitude environment, but also can provide data for broadening the application of BDS in the global wide.

For evaluating the performance of BDS in Arctic environments, the GNSS quality has been analyzed comprehensively in terms of SNR, MP, and other indicators. The experimental data from the International GNSS Service (IGS) stations in the terrestrial Arctic but not the Arctic Ocean (Lu et al., 2011). Du et al. (2015), Yang and Xu (2016) used measurements from an Antarctic, but the performance of PPP was not analyzed. This paper aims to evaluate the signal quality of BDS and the quality of PPP in the Arctic region and high latitude oceans using data collected by the Sinan receiver aboard the *Xuelong* icebreaker from the 9th China Arctic Science Study (July 20, 2018 to September 11, 2018).

A GNSS user not only needs high-precision positioning results, but also the reliability of the results. Thus, it is important to assure the integrity of PPP. When an external check condition is available for the measurement environment, the PPP result can be compared with an external known point or other high-precision positioning results, such as the real-time kinematic (RTK) positioning result. However, in the Arctic Ocean, where there is an absence of external check conditions, ensuring the reliability of PPP results is a challenge. The measurement method, baseline difference method, as well as the half-analysis method were used to assess the reliability of PPP positioning results (Yan et al., 2012). Unfortunately, these methods are mainly used for post-static processing. Guo (2013) proposed three PPP quality inspection methods include speed/acceleration test, forward-backward filter test, and GNSS inter-system test. These methods can determine whether there is an abnormality in the dynamic positioning result, but these methods cannot evaluate the accuracy of the positioning result. Receiver autonomous integrity monitoring (RAIM), which allows the system to timely alert the user to any failure or error in the navigation and positioning system (Lee, 1986, 2006; Wang et al., 2018). The protection level method based on RAIM was adopted to evaluate the integrity of GNSS (Miguel and Joaquin, 2009; Merino and Lainez, 2012; Madrid et al., 2015a, b). The protection level method performs well in the normal open-sky environment. As data may contain gross errors in harsh environment, it is difficult to determine the performance of protection level method in the marine environment. This paper adopts the RAIM-based protection level method and applies it to the quality check of PPP results. In view of that the observation data may contain gross errors and unmodeled errors in the marine environment, this paper uses median filter to improve the isotropy-based protection level algorithm. The accuracy and reliability of PPP positioning can be calculated by adopting the proposed method, which can provide reliable accuracy guarantee for marine applications in the mid-latitude oceanic region and in the Arctic Ocean.

The rest of the paper continues with the theory of PPP and the indicator of data quality analysis in Section 2. The improved protection level algorithm are explained and verified by the IGS station of Tixi experiment in Section 3. The BDS3 data quality and the positioning performance of PPP in the Arctic region are explained in Section 4. Finally, the conclusions are summarized in Section 5.

2 Theory

The PPP method was proposed by Zumberge et al. (1997) and it can provide centimeter to decimeter accuracy with the IGS precise products and advanced GPS error calibration methods.

2.1 *Function model*

The classical PPP function models include the ionospheric-free combination model (Zumberge et al., 1997), the UofC model (Gao and Shen, 2002) and the uncombined model (Abdel-Salam, 2005).

GNSS raw pseudorange and carrier phase observation equations are defined as

$$\begin{cases} P_{i,r}^{j} = \rho_r^j + \delta t_r - \delta t^j + d_{\text{orb}}^j + T_r^j + \gamma_i I_{1,r}^j + \\ d_{i,r} - d_i^j + \varepsilon(P_{i,r}^j), \\ L_{i,r}^{j} = \rho_r^j + \delta t_r - \delta t^j + d_{\text{orb}}^j + T_r^j - \gamma_i I_{1,r}^j + \\ b_{i,r} - b_i^j + \lambda_i N_{i,r}^j + \varepsilon(L_{i,r}^j), \end{cases} \tag{1}$$

where $L_{i,r}^j$ and $P_{i,r}^j$ are the raw carrier phase and pseudorange observation in meters; the superscript j denotes the satellite number; the subscript r is the station number, and i indicates the carrier frequency. ρ_r^j is the geometric distance between the antenna phase center of the receiver and the antenna phase center of the satellite; δt_r and δt^j are the receiver clock error and satellite clock error respectively. $T_r^j$is the tropospheric delay, and $I_{1,r}^j$ is the ionospheric delay of the first carrier frequency with $\gamma_i = f_1^2/f_2^2$. $d_{i,r} d_i^j$ and $b_{i,r} b_i^j$are the receiver and satellite pseudorange and carrier phase hardware delay, respectively; $N_{i,r}^j$ is the ambiguity parameter; λ_i is the carrier wavelength of carrier frequency i. $\varepsilon(L_{i,r}^j)$ and $\varepsilon(P_{i,r}^j)$ are the noise of the carrier phase and pseudorange observations. The geometric distance between the station and the satellite ρ_r^j can be further expressed as:

$$\rho_r^j = \sqrt{(x^j - x_r)^2 + (y^j - y_r)^2 + (z^j - z_r)^2}, \tag{2}$$

where $(x^j, y^j, z^j)^{\mathrm{T}}$ is the position of the satellite, which can be obtained from the precise ephemeris, and $(x_r, y_r, z_r)^{\mathrm{T}}$ is the position of the receiver to be estimated.

In order to eliminate the first-order term of ionospheric delay, the ionospheric-free combination is employed. In this case, the ionospheric-free combinations of the pseudorange and carrier phase observation equations are expressed as

$$\begin{cases} P_{\text{IF},r}^j = \dfrac{f_1^2 \cdot P_{1,r}^j - f_2^2 \cdot P_{2,r}^j}{f_1^2 - f_2^2} = \rho_r^j + (\delta t_r + d_{\text{IF},r}) - \\ \qquad (\delta t^j + d_{\text{IF}}^j) + d_{\text{orb}}^j + T_r^j + \varepsilon(P_{\text{IF},r}^j), \\ L_{\text{IF},r}^j = \dfrac{f_1^2 \cdot L_{1,r}^j - f_2^2 \cdot L_{2,r}^j}{f_1^2 - f_2^2} \\ \qquad = \rho_r^j + (\delta t_r + d_{\text{IF},r}) - (\delta t^j + d_{\text{IF}}^j) + d_{\text{orb}}^j + T_r^j + \\ \qquad (b_{\text{IF},r} - d_{\text{IF},r} + d_{\text{IF}}^j - b_{\text{IF}}^j + \lambda_{\text{IF}} N_{\text{IF},r}^j) + \varepsilon(L_{\text{IF},r}^j), \end{cases} \tag{3}$$

where the subscript IF indicates the ionospheric-free combination, and the other symbols are the same as before.

2.2 *Kalman filter*

After the PPP observation equations are formed, Kalman filter is used to estimate the unknown parameters. Kalman filter uses a recursive algorithm that combines the estimated state vector of the previous epoch and the observations of the current epoch to estimate the current state (Xiao et al., 2018). The state vector consists of the parameters to be estimated in the PPP observation equation. The filtered state equation and observation

equation are shown as

$$\begin{cases} \boldsymbol{V}_{\bar{\boldsymbol{X}}_k} = \hat{\boldsymbol{X}}_k - \bar{\boldsymbol{X}}_k, \\ \boldsymbol{V}_k = \boldsymbol{A}_k \hat{\boldsymbol{X}}_k - \boldsymbol{L}_k, \end{cases} \tag{4}$$

where $\hat{\boldsymbol{X}}_k$ is the estimated state vector at time k, subscript is the current epoch k. $\hat{\boldsymbol{X}}_k$ is the vector of parameters to be estimated , which usually contains position parameters and other parameters . In general, the parameter vector to be estimated can be expressed as $(x, y, z, \delta t_r, \cdots)$. $\sum_{\hat{\boldsymbol{X}}_k}$ is the covariance matrix, which can be expressed as $\begin{pmatrix} \sigma_{xx} & & & \\ & \sigma_{yy} & & \\ & & \sigma_{zz} & \\ & & & \sigma_{\delta t_r \delta t_r} \end{pmatrix}$. $\bar{\boldsymbol{X}}_k$ is the predicted state vector at time k and $\sum_{\bar{\boldsymbol{X}}_k}$ is the covariance. $\boldsymbol{V}_k$ is the residual vector of $\boldsymbol{L}_k$; $\boldsymbol{V}_{\bar{\boldsymbol{X}}_k}$ is the residual vector of $\bar{\boldsymbol{X}}_k$. $\boldsymbol{A}_k$ is the modulus matrix; $\boldsymbol{L}_k$ is the observation vector.

Given initial values of filtered state vector $\hat{\boldsymbol{X}}_0$ and variance $\sum_0$, the estimated state vector at time k can be calculated recursively. The predicted state vector $\bar{\boldsymbol{X}}_k$ at time $k$and its covariance $\sum_{\bar{\boldsymbol{X}}_k}$ are determined as

$$\begin{cases} \bar{\boldsymbol{X}}_k = \Phi_{k,k-1} \hat{\boldsymbol{X}}_{k-1}, \\ \sum_{\bar{X}_k} = \Phi_{k,k-1} \sum_{\hat{X}_{k-1}} \Phi_{k,k-1}^{\mathrm{T}} + Q_{k-1}. \end{cases} \tag{5}$$

The estimated state vector $\hat{\boldsymbol{X}}_k$ at time k and its covariance matrix $\sum_{\hat{\boldsymbol{X}}_k}$ are shown as

$$\begin{cases} \hat{\boldsymbol{X}}_k = (\boldsymbol{A}_k^{\mathrm{T}} P_k \boldsymbol{A}_k + P_{\bar{\boldsymbol{X}}_k})^{-1} (\boldsymbol{A}_k^{\mathrm{T}} P_k \boldsymbol{L}_k + P_{\bar{\boldsymbol{X}}_k} \bar{\boldsymbol{X}}_k), \\ \sum_{\hat{\boldsymbol{X}}_k} = \sum_{\bar{\boldsymbol{X}}_k} - \sum_{\bar{\boldsymbol{X}}_k} \boldsymbol{A}_k^{\mathrm{T}} \left(\boldsymbol{A}_k \sum_{\bar{\boldsymbol{X}}_k} \boldsymbol{A}_k^{\mathrm{T}} + \sum_k \right)^{-1} \boldsymbol{A}_k \sum_{\bar{\boldsymbol{X}}_k}, \end{cases} \tag{6}$$

where $\hat{\boldsymbol{X}}_{k-1}$ and $\sum_{\hat{\boldsymbol{X}}_{k-1}}$ are estimated state vector and their variance matrices at time $k-1$. $P_{\bar{\boldsymbol{X}}_k} = \sum_{\bar{\boldsymbol{X}}_k}^{-1}$, P_k is the weight matrix of the observation.

2.3 *PPP strategy*

PPP uses ionospheric-free combination model and Kalman filter to estimate parameters. Data is processed by self-developed software, which based on the Visual Studio 2017 platform with the C/C++ language. The detailed parameter estimation strategy, the initial value of the filter, and the processing strategies are shown in Table 1.

2.4 *Quality analysis of satellite signal*

The quality of the satellite signal has an important impact on the positioning results. In order to comprehensively analyze the positioning performance of BDS3 in the Arctic Ocean, this paper uses five indicators to analyze the satellite signal quality: number of visible satellites, SNR, MP, DOP and code-minus-carrier combination (CC).

2.4.1 *Number of visible satellites*

The continuous visibility of satellites can ensure the convergence of position parameters in PPP. Generally speaking, if the number of visible satellites is greater than 4, the positional parameters can be effectively converged (Geng et al., 2009).

2.4.2 *SNR*

SNR is one of the most important indicators of satellite signal quality. The higher the value of SNR, the better the quality of the corresponding observed signal.

2.4.3 *MP*

Satellite receivers not only receive signals directly from satellites, but also receive satellite signals reflected by objects (such as water surfaces, buildings, ...). If the received signal is reflected by several reflector surfaces, the signal will affect the accuracy of positioning. MP is an important factor that affecting the precision of PPP. The MP combination observation formula is as follows:

Table 1. PPP parameter configuration

Processing item	Processing strategy
Observation	dual-frequency carrier phase and pseudorange observations, ionospheric-free combination model
Cutoff angle	10°
Satellite DCB	differential code bias (DCB) products released by Center for Orbit Determination in Europe and Multi-GNSS Experiment
Antenna phase center correction	BeiDou satellite: estimated value provided by European Space Agency Receiver: igs_14.atx model
Phase windup effect	model correction
Tidal corrections	solid tides, tides and pole tide corrections
Relativistic effect	model correction
Earth orientation parameter	fixed to International Earth Rotation Service result
Satellite position and satellite clock	Precision ephemeris products provided by Geo Forschungs Zentrum
Station position	static/kinematic, parameter estimation
Receive clock	white noise estimation, process noise is $8.1\mathrm{e}^7$ $\mathrm{m}^2/\mathrm{s} \times \Delta t$ the initial value is obtained from the estimation of pseudorange, the initial variance is $9\mathrm{e}^6$ m^2
Tropospheric delay	dry component, using University of New Brunswick 3 model correction wet component, estimated by a random walk process the process noise is $3\mathrm{e}^{-8}$ $\mathrm{m}^2/\mathrm{s} \times \Delta t$ the initial value is given by the model and the initial variance is 0.25 m^2
Ionospheric delay	ionospheric-freecombination model
Ambiguity	estimated as a constant value and reset when a cycle slip occurs

$$\begin{cases} \mathrm{MP}^j_{i,r} = P^j_{i,r} - \dfrac{f_i^2+f_k^2}{f_i^2-f_k^2}\lambda_i\varphi^j_{i,r} + \dfrac{2f_k^2}{f_i^2-f_k^2}\lambda_k\varphi^j_{k,r} - B^j_{i,r}, \\ B^j_{i,r} = -\dfrac{f_i^2+f_k^2}{f_i^2-f_k^2}\lambda_i N^j_{i,r} + \dfrac{2f_k^2}{f_i^2-f_k^2}\lambda_k N^j_{k,r} + (d_{i,r} - d^j_i), \end{cases} \tag{7}$$

where $\mathrm{MP}^j_{i,r}$ is the MP of frequency i, $B^j_{i,r}$ is the float ambiguity which can be obtained by multi-epoch data smoothing. The other symbols are the same as before.

2.4.4 *The geometry of constellations*

The GNSS positioning accuracy is not only determined by the ranging accuracy, but also by the geometry of constellations (Wang et al., 2019). Geometrical dilution of precision (GDOP), Positional dilution of precision (PDOP), Horizontal dilution of precision (HDOP) and Vertical dilution of precision (VDOP) are selected as the index for assessing the quality of satellite geometric distribution. The formula is shown as:

$$\begin{cases} \mathrm{GDOP} = \sqrt{\sigma_{xx}+\sigma_{yy}+\sigma_{zz}+\sigma_{\delta t_r \delta t_r}}, \\ \mathrm{PDOP} = \sqrt{\sigma_{xx}+\sigma_{yy}+\sigma_{zz}}, \\ \mathrm{HDOP} = \sqrt{\sigma_{xx}+\sigma_{yy}}, \\ \mathrm{VDOP} = \sqrt{\sigma_{zz}}, \end{cases} \tag{8}$$

the symbols are the same as before.

2.4.5 *Pseudorange noise analysis*

Pseudorange noise indicates the basic performance of GNSS receiver, which is usually calculated by the CC. The formula of CC is shown as (Xu et al., 2018)

$$\mathrm{CC}^j_{i,r} = P^j_{i,r} - L^j_{i,r}, \tag{9}$$

the symbols are the same as before.

The CC performs the difference between the epochs, which can eliminates the carrier phase ambiguity and reduces the error such as ionospheric delay, hardware delay, and multipath. The residual part is mainly affected by pseudorange noise.

3 Quality inspection

Integrity is the measure of the trust that can be placed in the correctness of the information supplied by navigation system. Integrity includes the ability of the system to provide timely warnings to users when the system should not be used for navigation (Merino and Lainez, 2012). To ensure the safety and reliability of GNSS, GNSS integrity monitoring can be divided into system-level integrity monitoring and user-level integrity monitoring. User-level integrity monitoring, also known as RAIM. As an important part of RAIM, the user's protection level is calculated based on redundant observations to monitors the integrity of user positioning result. This study adopts the RAIM-based protection level method for checking the reliability and the positioning accuracy of PPP.

3.1 *The protection level method*

The protection level is computed using the statistical bound error so as to guarantee that the probability of the absolute position error exceeding the said number is smaller than or equal to the target integrity risk (Merino and Lainez, 2012). The integrity risk is the risk that the position error exceeds the alert limit at any moment. The PL is divided into horizontal protection level (HPL) and vertical protection level (VPL). There are two ways to calculate the protection level. One way uses the variance information of the positional parameter, while the other way uses the posterior residual information (Feng et al., 2009).

The variance-based protection level can be expressed as

$$\begin{cases} \mathrm{HPL} = k_H\sigma_H, \sigma_H = \sqrt{\sigma_{xx}+\sigma_{yy}}, \\ \mathrm{VPL} = k_U\sigma_U, \sigma_U = \sqrt{\sigma_{zz}}, \end{cases} \tag{10}$$

where k_H and k_U are factors that obey a normal distribution , and they can be determined according to the integrity risk. σ_H and σ_U are the middle errors in the horizontal and vertical directions respectively. σ_{xx}, σ_{yy} , σ_{zz} are element in the parameter variance matrix.

The isotropy-based protection level (IBPL) assumes that the space vector is composed of the observation error. Both the size and the direction are arbitrary in the vector space, which means there is no priori information and the difference after the adjustment will be reflected in the posterior residual. The isotropy-based protection levels can be expressed as (Miguel and Joaquin, 2009)

$$\begin{cases} \mathrm{HPL} = k_{\mathrm{IBPL}}\,\|V\|\,\sigma_H, \sigma_H \\ \qquad = \sqrt{\dfrac{\sigma_{xx}+\sigma_{yy}}{2} + \sqrt{\left(\dfrac{\sigma_{xx}-\sigma_{yy}}{2}\right)^2 + \left(\dfrac{\sigma_{xx}+\sigma_{yy}}{2}\right)^2}}, \\ \mathrm{VPL} = k_{\mathrm{IBPL}}\,\|V\|\,\sigma_U, \sigma_U = \sqrt{\sigma_{zz}}, \end{cases} \tag{11}$$

where $\|V\|$ is the euclidean distance of the posterior residual and k_{IBPL} can be obtained according to the integrity risk checklist.

As isotropy-based protection level makes full use of the posterior residual information, it can reflect the undetected gross error. However, the variance-based protection level does not take advantage of the posterior residual information.

3.2 *Experiment*

The reliability and the accuracy of the protection level need to be verified by experiment. It is important to choose a suitable experiment station, which must meet two requirements. First, the measurement environment of station should be similar to the Arctic marine environment. Second, the station should have a high-precision external inspection standard. Based on the above requirements, the IGS station of Tixi was selected, which has known high precise coordinates. Experiment downloaded Tixi Station data of August 3, 2018 from the IGS website. Then the data was used to calculate the variance-based protection level and the isotropy-based protection level. The positional bias was obtained from the difference between the PPP result in pseudo-kinematic mode and the known coordinates of the IGS station with high precision.

Figure 1 shows the relationship between the PPP positional bias and the variance-based protection level, while Fig. 2 shows the relationship between the PPP positional bias and the isotropy-based protection level. The green lines in Figs 1a and 2a represent the PPP positional bias in north and east direction. The blue line in Fig. 1a represents the horizontal variance-based protection level calculated by Eq. (10), in which k_H is 6.18. The red line in Fig. 2a represents the horizontal isotropy-based protection level calculated by Eq. (11), in which the confidence level is set to 99.9% (Miguel and Joaquin, 2009). Moreover, the green line in Fig. 1b represents the PPP positional bias in up direction. The blue line in Fig. 1b represents the vertical variance-based protection level calculated by Eq. (10), in which k_U is 5.33 . The red line in Fig. 2b represents the vertical isotropy-based protection level

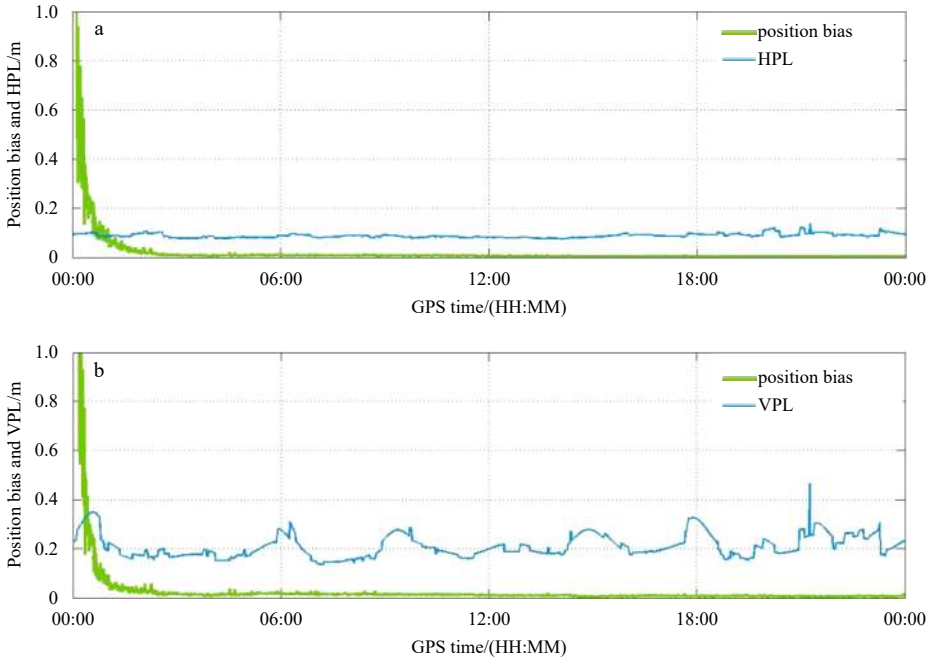

Fig. 1. Horizontal variance-based protection level of Tixi Station (a), and vertical variance-based protection level of Tixi Station (b).

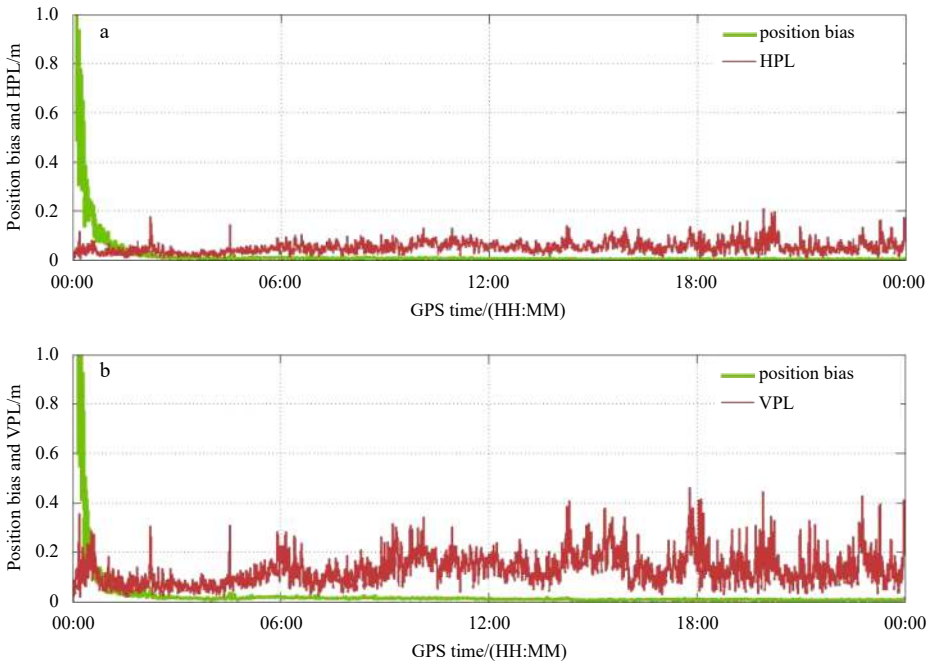

Fig. 2. Horizontal isotropy-based protection level of Tixi Station (a), and vertical isotropy-based protection level of Tixi Station (b).

calculated by Eq. (11), in which the confidence level is set to 99.9% (Miguel and Joaquin, 2009).

From Figs 1 and 2, it can be seen that there are short-term fluctuations at the beginning under the pseudo-kinematic conditions. However, all the position biases are below the protection level after a few hours, which means that the protection level calculated by the two methods can well define the position bias of PPP.

As residuals can reflect anomalies effectively, the isotropy-based protection level can reflect the influence of the gross errors on the positioning result theoretically. In view of observation data contains gross errors easily in the marine environment, an experiment involving gross errors was carried out. A gross error of 0.6 m was added to the carrier observation of the satellites every three hours during the PPP filter process in the test.

Figure 3 shows the relationship between the positional bias of the PPP and the variance-based protection level in the horizontal and vertical directions. Figure 4 shows the relationship between the positional bias of the PPP and the isotropy-based protection level in the horizontal and vertical directions. Both experiments were conducted under pseudo-kinematic conditions with a gross error of 0.6 m every three hours.

The green lines represent the positional biases of PPP in Figs 3 and 4. Due to the gross error of 0.6 m added to the carrier obser-

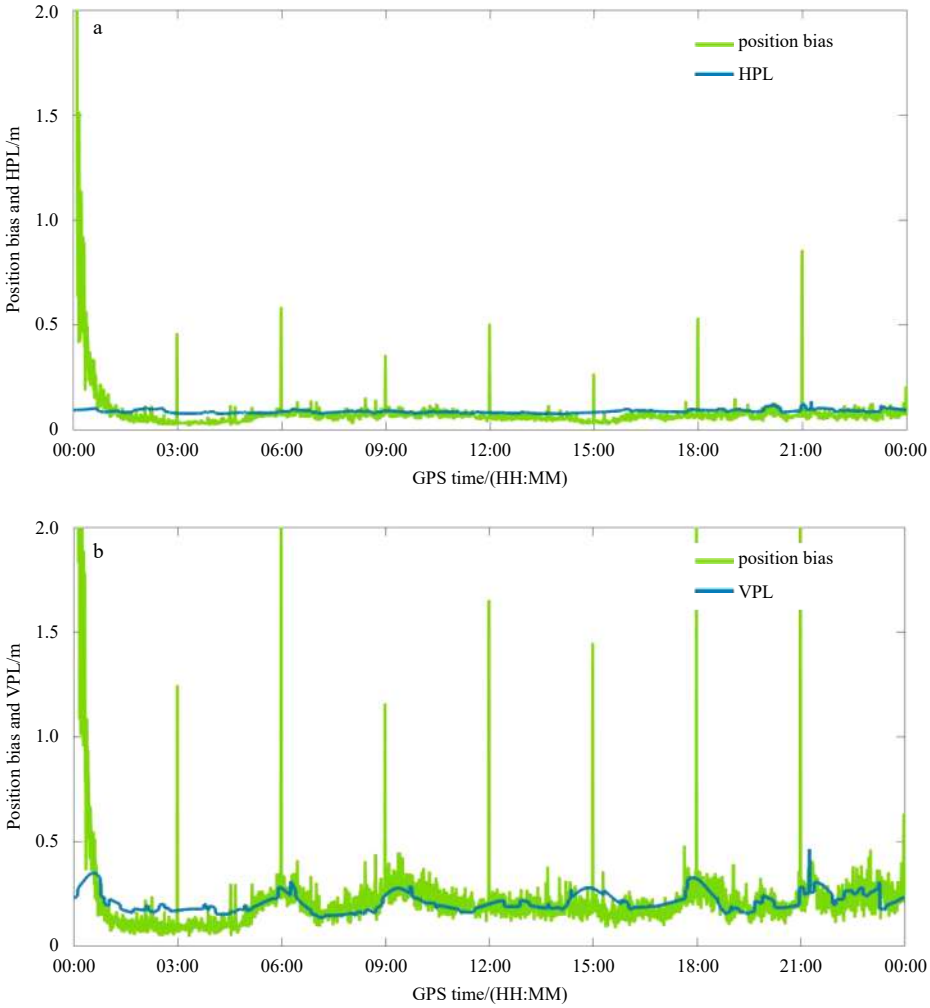

Fig. 3. Horizontal variance-based protection level of Tixi Station (artificially added gross errors) (a), and vertical variance-based protection level of Tixi Station (artificially added gross errors) (b).

vation every three hours, the positional biases of PPP jump at the corresponding times. The red lines represent the isotropy-based protection level. The isotropy-based protection level show a large fluctuation every three hours, which caused by the gross error. The blue lines represent the variance-based protection level, and the variance-based protection level has no obvious fluctuations. Overall, the variance-based protection level is flat rather than unusually volatile. This is mainly because this method does not make full use of the post-test residual information of the observation. In general, the protection level in the case of artificially added errors is worse than the protection level without artificially added errors. Moreover, compared with the variance-based protection level, the isotropy-based protection level reflects the existence of gross errors better.

The isotropy-based protection level is roughly equal to the position bias in the horizontal direction. The isotropy-based protection level deviates from the position bias in the vertical direction, that is, the protection level is lower than the position bias. In this case, the protection level cannot reflect the position biases accurately. This is mainly because of the influence of the unmodeled errors in PPP such as residual ephemeris errors and MP. The errors are reflected in the posterior residual, which makes the protection level sequence fluctuate significantly.

The measurement environment is unstable and the observation data is susceptible to the gross errors and unmodeled errors in the marine environment. This paper proposes an improved isotropy-based protection level algorithm, which uses median filter to eliminate the influence of gross error. The improved protection level not only can reflect the fluctuation of gross error, but also can reflect the level of positional bias well.

3.3 *Improved isotropy-based protection level algorithm*

Considering the characteristics of the gross error, this paper uses a nonlinear algorithm based on median filter to smooth the euclidean distance of the posterior residual. The algorithm can improve the fluctuation of the isotropy-based protection level.

Median filter is a nonlinear signal processing technique based on sorting statistics, which can suppress isolated noise effectively. The basic principle of median filter involves first sorting the signals, followed by determining the sorting window size and sorting the signal values according to the window center point, and finally taking the middle value as the new value of the center signal. When the window moves, the signal can be smoothed by median filter to eliminate isolated noise points.

Suppose that the posterior residual euclidean distance of the i epoch is V_i, and the window size of the median filter is n, then the median filter variables at i epoch can be expressed as Median $V_i = (V_{i-n}, V_{i-n+1}, \cdots, V_{i-1}, V_i, V_{i+1}, V_{i+2}, \cdots, V_{i+n})$, the corresponding order statistics $V_{(i-n)} \leqslant V_{(i-n+1)} \leqslant \cdots \leqslant V_{(i)} \leqslant \cdots \leqslant V_{(i+n-1)} \leqslant V_{(i+n)}$ are random variables. The values of V_i sorts in an ascend-

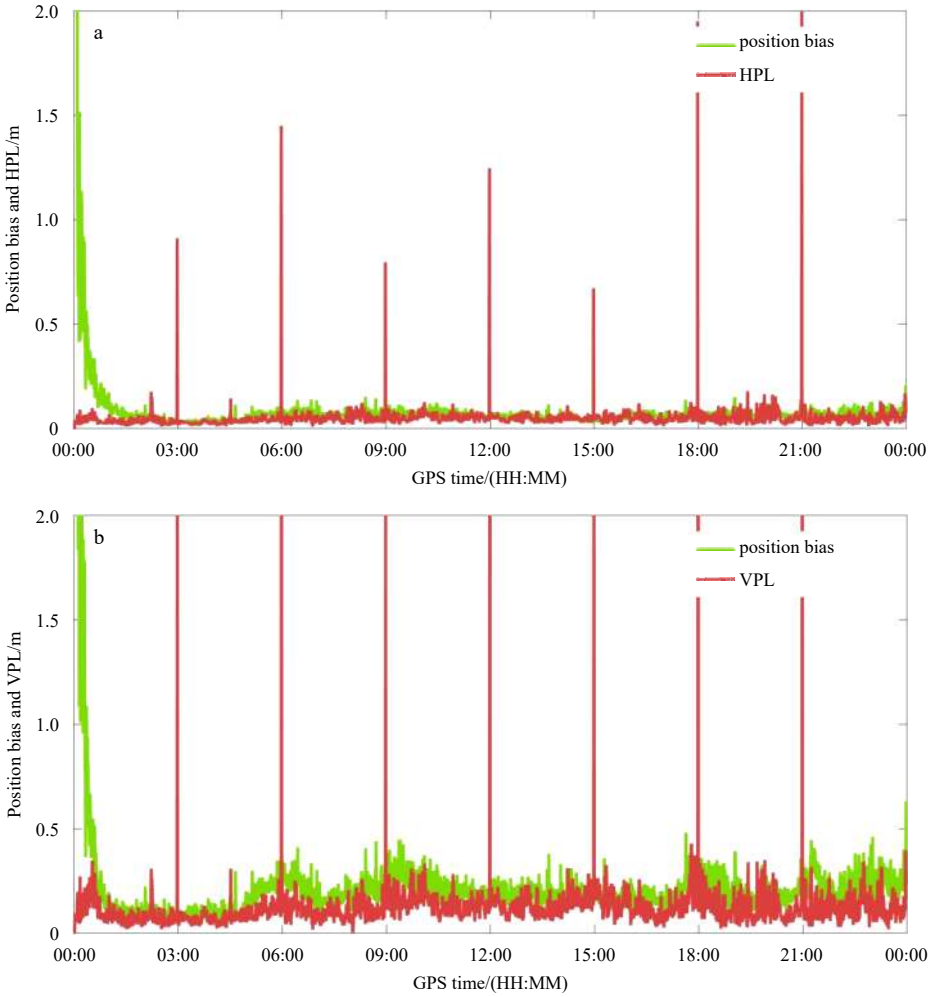

Fig. 4. Horizontal isotropy-based protection level of Tixi Station (artificially added gross errors) (a), and vertical isotropy-based protection level of Tixi Station (artificially added gross errors) (b).

ing order, then the median value of V_i is given as

$$\text{Median}V_i = \begin{cases} V_{(2k+1)}, n = 2k, \\ \dfrac{V_{(2k)} + V_{(2k+1)}}{2}, n = 2k+1. \end{cases} \tag{12}$$

The steps of the improved isotropy-based protection level algorithm are presented as follows: (1) median filter is used to smooth the window of the posterior residual euclidean distance of n epochs and the value of n is usually set to [5, 20]; (2) use the Eq. (12) to calculate the median value of posterior residual euclidean distance and take it as the current posterior residual euclidean distance estimate; (3) use the current post-test residual euclidean distance estimate to calculate the isotropy-based protection level.

Figure 5 shows the relationship of the positional biases of PPP, the isotropy-based protection level, and the improved isotropy-based protection level in the horizontal and vertical directions. The experiment uses the data from Tixi Station and adopts pseudo-kinematic mode. The green lines represent the PPP positional bias. The red lines represent the isotropy-based protection level, and the improved isotropy-based protection level algorithm is represented by purple lines.

In Fig. 5, the purple lines are always above the green lines, which indicates the improved isotropy-based protection level algorithm can reflect the positioning precisely. Compared with the isotropy-based protection level algorithm, the improved algorithm produces result closer to the PPP position bias. Therefore, the improved isotropy-based protection level is more suitable for evaluating the position quality of dynamic PPP in Arctic Oceanic region.

4 Arctic Ocean experiment

This study uses the data from the Sinan receiver mounted on the *Xuelong* icebreaker during the 9th China Arctic Science Study (July 20, 2018–September 11, 2018). The *Xuelong* icebreaker is the only Chinese icebreaker to mount a full scientific expedition of the polar regions. The data sampling rate is 1 s, and the height cutoff angle is 10°. The *Xuelong* icebreaker sailed for 53 days, and the highest latitude of the track reached 84.22° to the north. The *Xuelong* icebreaker is shown in Fig. 6. The expedition track is shown by the red line in Fig. 7.

In order to analyze the signal quality of BDS in the Arctic Ocean at different latitudes, representative data from Day of Year (DOY) 204 with latitude around 45°, DOY 209 with latitude around 60°, and DOY 215 with latitude around 75°, were selected. The collected datasets were processed to compare the number of visible satellites, SNR, MP, DOP and CC of BDS at different latitudes. The numbers of visible satellites at different latitudes are

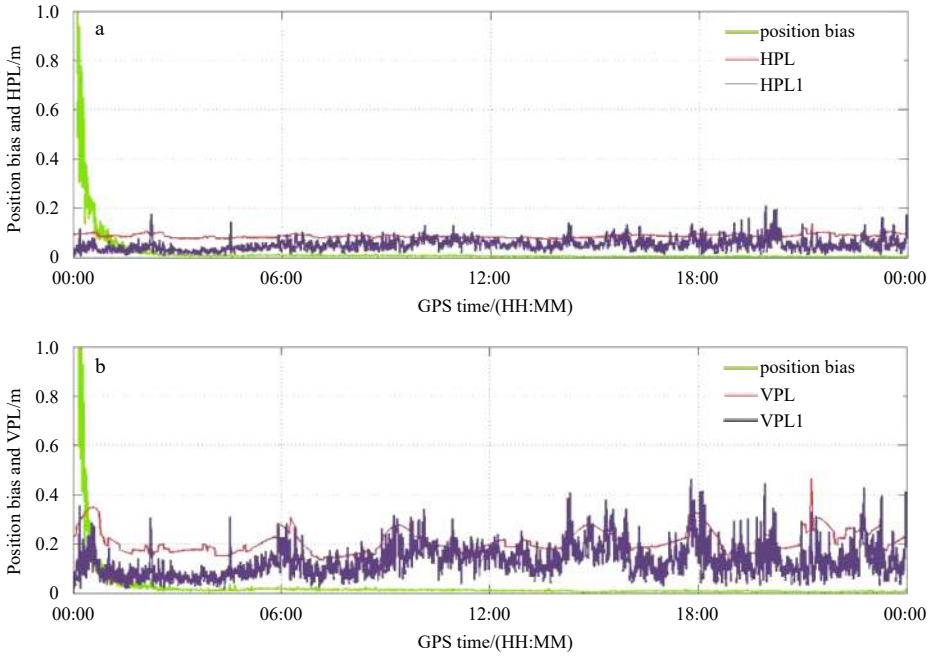

Fig. 5. Relationship between position bias and protection level before and after IBPL algorithm improvement of Tixi Station data (horizontal) (a); relationship between position bias and protection level before and after IBPL algorithm improvement of Tixi Station data (vertical) (b).

Fig. 6. *Xuelong* icebreaker.

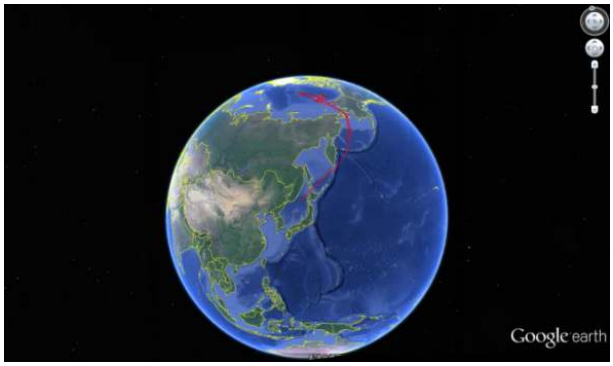

Fig. 7. *Xuelong* Polar expedition track map.

shown in Fig. 8.

In Fig. 8, the blue lines represent the visible time period of the BeiDou 2nd generation satellite, while the red lines represent the visible time period of the BeiDou 3rd generation satellite. The number of visible BeiDou satellites is 8–13 at 45° latitude, 6–11 at 60° latitude and 5–8 at 75° latitude. This shows that more than 4 BDS satellites can be observed at any time in the mid-high latitude ocean area, which can ensure the positioning accuracy effectively.

The SNR and MP results with respect to the elevation angle for the different latitudes are shown in Fig. 9.

From Fig. 9, it can be seen that the value range of SNR is [25, 52]dB Hz in the mid-latitude and high-latitude ocean regions. The data shows that the signal quality is quite good throughout the journey. As the elevation angle increases, the value of SNR increases slowly. The value range of MP is [–2, 2] m, which is not significantly different with the increase in latitude. The value of MP tends to decrease slowly as the elevation angle increases.

The geometry of the constellations for the different latitudes are shown in Fig. 10.

From Fig. 10, it can be seen that the value of geometric precision factor is similar in 45° latitudes and 60° latitudes ocean. Taking the value of GDOP as an example, most of the values are below 3. However, the value of GDOP is much larger in 70° latitudes ocean and the maximum is even reach to 7. This means that in the high latitudes, the BeiDou satellite geometry distribution is not as good as that in the mid-latitude area. BDS is still under construction, and it is expected to provide a more promising service on a global scale in the future.

Taking the B1I and BIC frequencies of C20 satellite as an example, the CC at the different latitudes are shown in Fig. 11.

From Fig. 11, it can be seen that the CC of B1I and BIC frequencies have a similar curve in different latitudes ocean. Generally speaking, the values of CC are between –5 m and 5 m, which means the effect of pseudorange noise is small.

The positioning strategy described in Section 2.3 was used to process the data, and the accuracy of PPP was calculated by the improved protection level. Due to the similar positioning accuracy at mid-high latitudes, data from DOY217 (the approximate

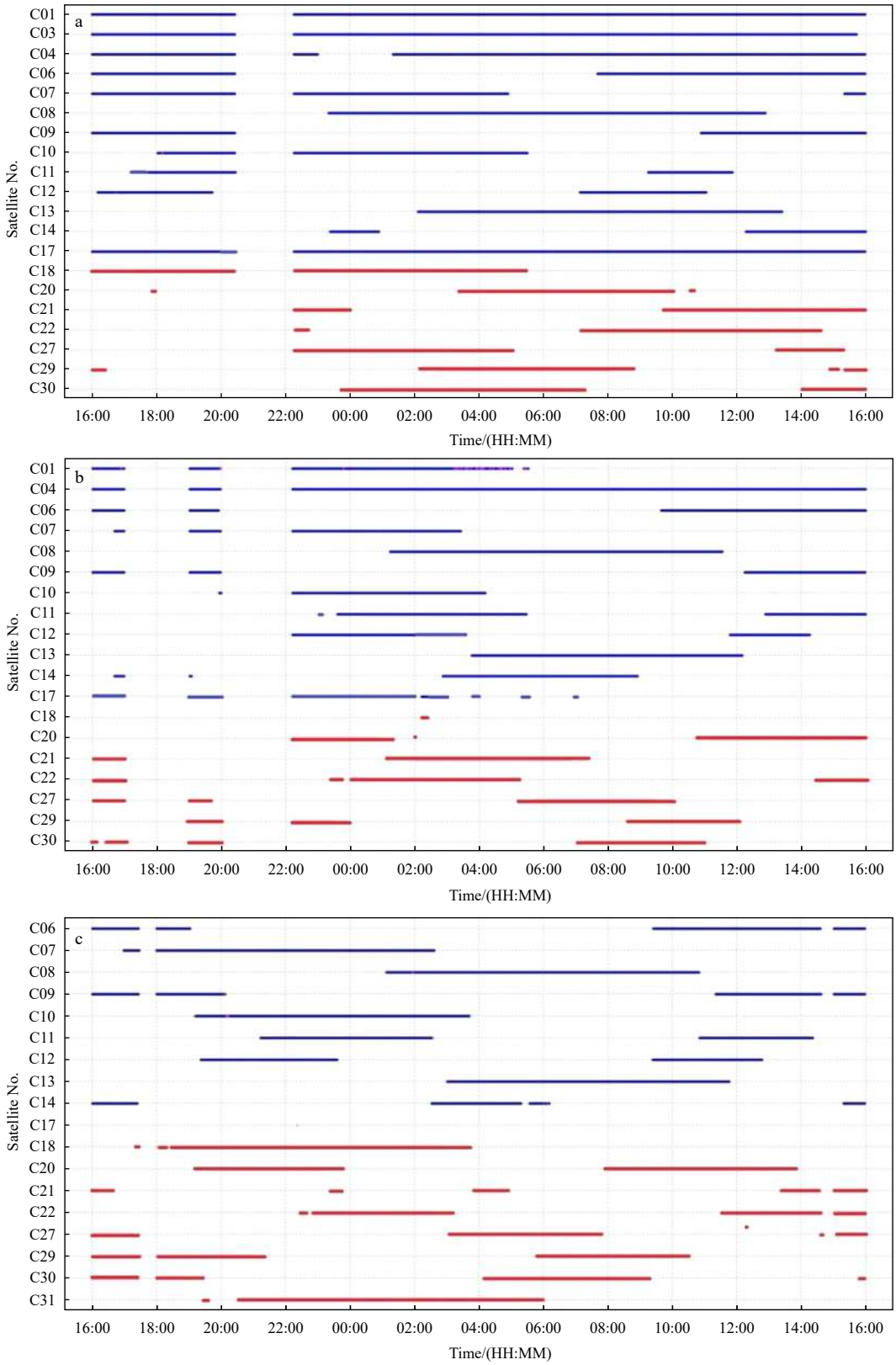

Fig. 8. Number of visible satellites of latitude around 45° (DOY 204) (a), number of visible satellites of latitude around 60° (DOY 209) (b), and number of visible satellites of latitude around 75° (DOY 215) (c).

location is located at 76.95°N, 171.90°E) was selected for analysis. The performance of PPP on DOY217 is shown in Fig. 12.

It can be seen from Fig. 12 that the improved isotropy-based protection level sometimes experiences drastic jumps. Due to the harsh Arctic marine environment, the observation may contain gross errors. The improved isotropy-based protection level ex-

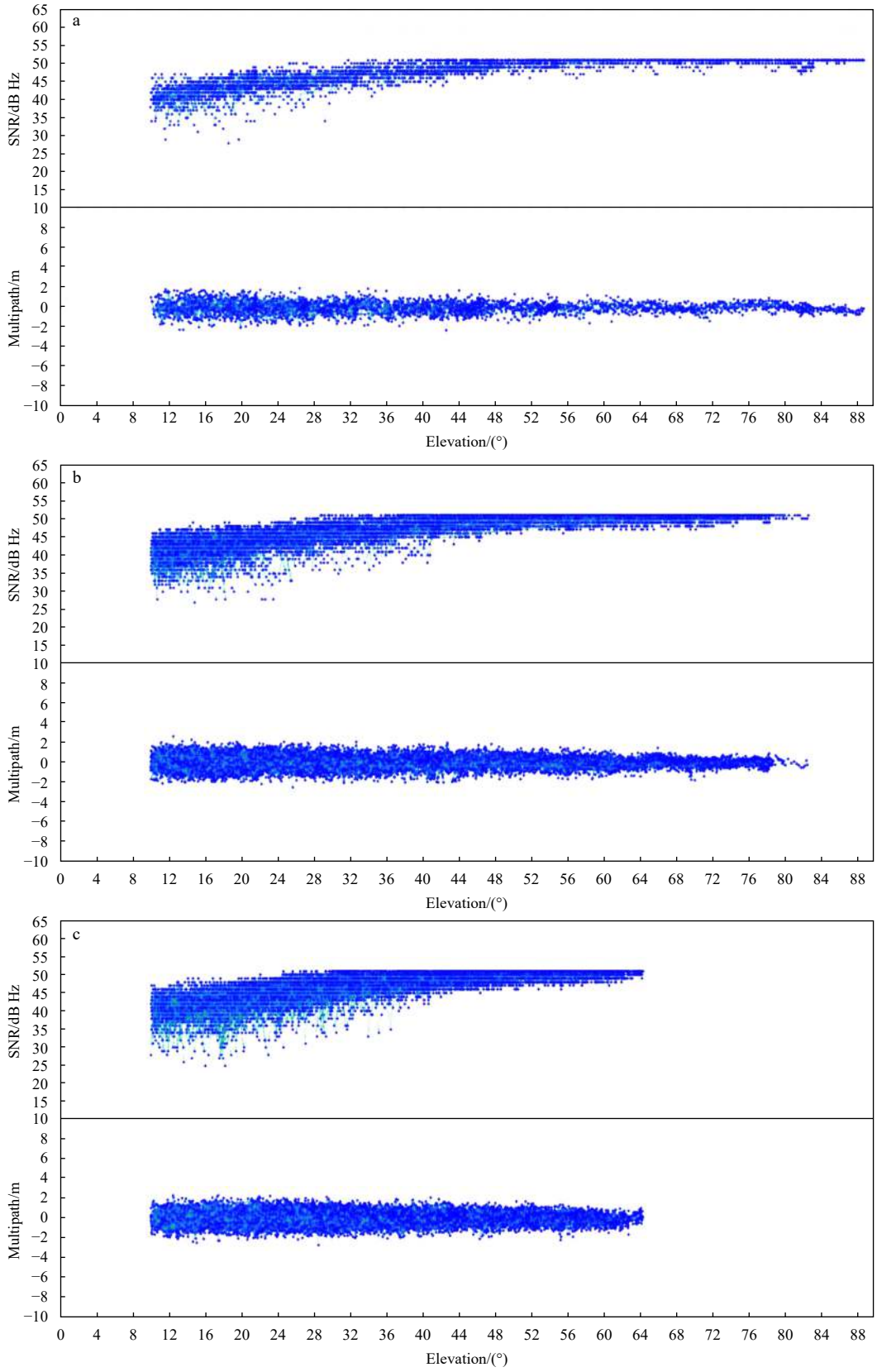

Fig. 9. Signal to noise ratio (SNR) and multiparth (MP) of latitude around 45° (DOY 204) (a), SNR and MP of latitude around 60° (DOY 209) (b), and SNR and MP of latitude around 75° (DOY 215) (c).

periences drastic fluctuations. This means that the improved isotropy-based protection level can reflect the gross errors reliably. More importantly, the improved isotropy-based protection level can reflect the precision of PPP. The improved isotropy-based

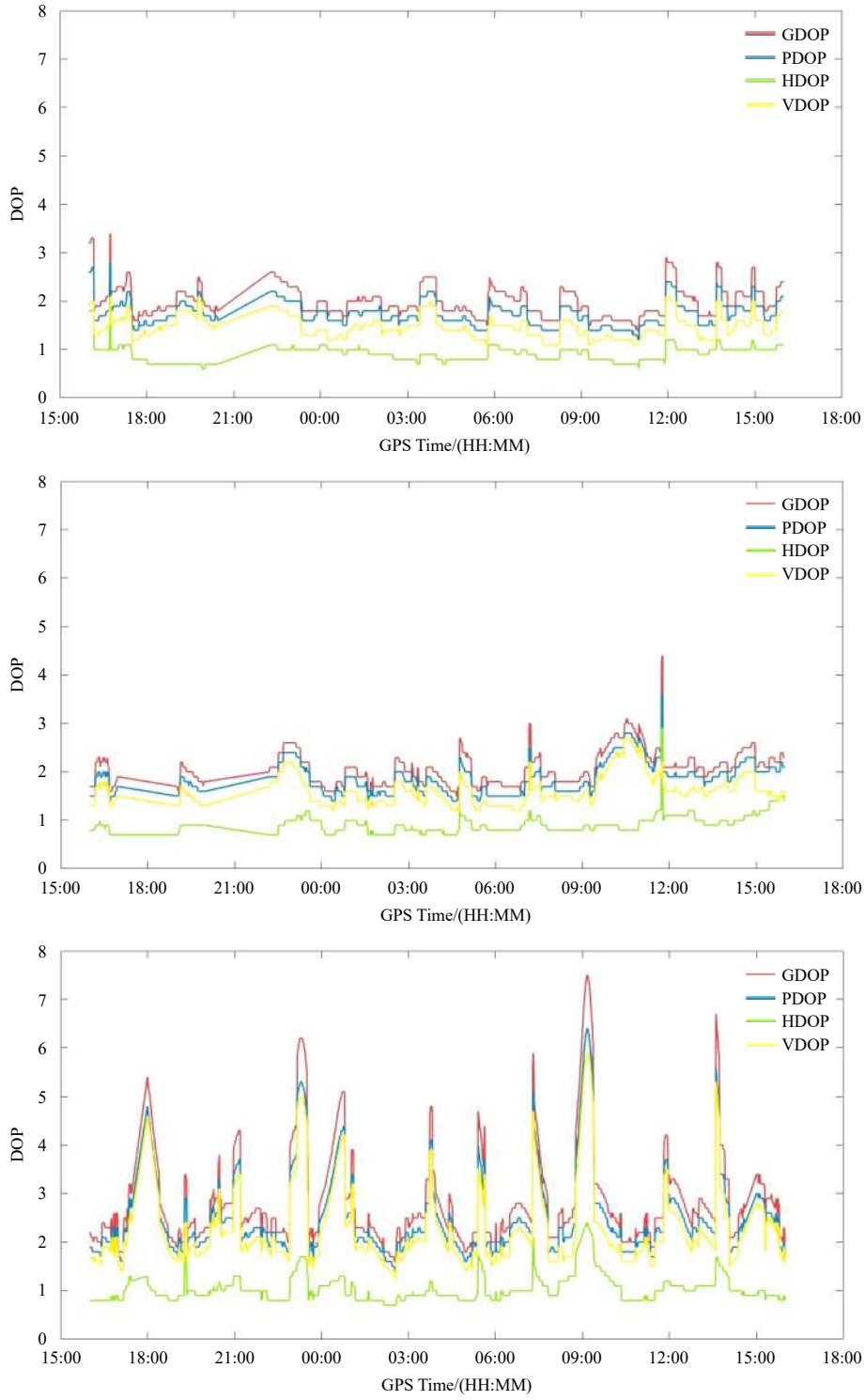

Fig. 10. Dilution of precision (DOP) of latitude around 45° (DOY 204) (a), DOP of latitude around 60° (DOY 209) (b), and DOP of latitude around 75° (DOY 215) (c).

protection level can reach the decimeter level in the horizontal and vertical direction, which means that the kinematic accuracy of PPP can reach the decimeter level in the Arctic Ocean and it meets the precision requirements of maritime navigation.

5 Conclusions

Based on the BDS3 data collected by the *Xuelong* icebreaker during the 9th China Arctic expedition, this paper analyzes the data quality and the PPP performance of BDS3 in the Arctic Ocean. The following conclusions are drawn:

(1) The numbers of visible BDS3 satellites are more than four at any time in the mid-latitude sea area and the Arctic Ocean, which can ensure BDS provide positioning services on a global scale.

(2) The values SNR of BDS3 signals range from 25 dB Hz to 52 dB Hz and the value range of MP is [–2, 2] m in the mid-latitude

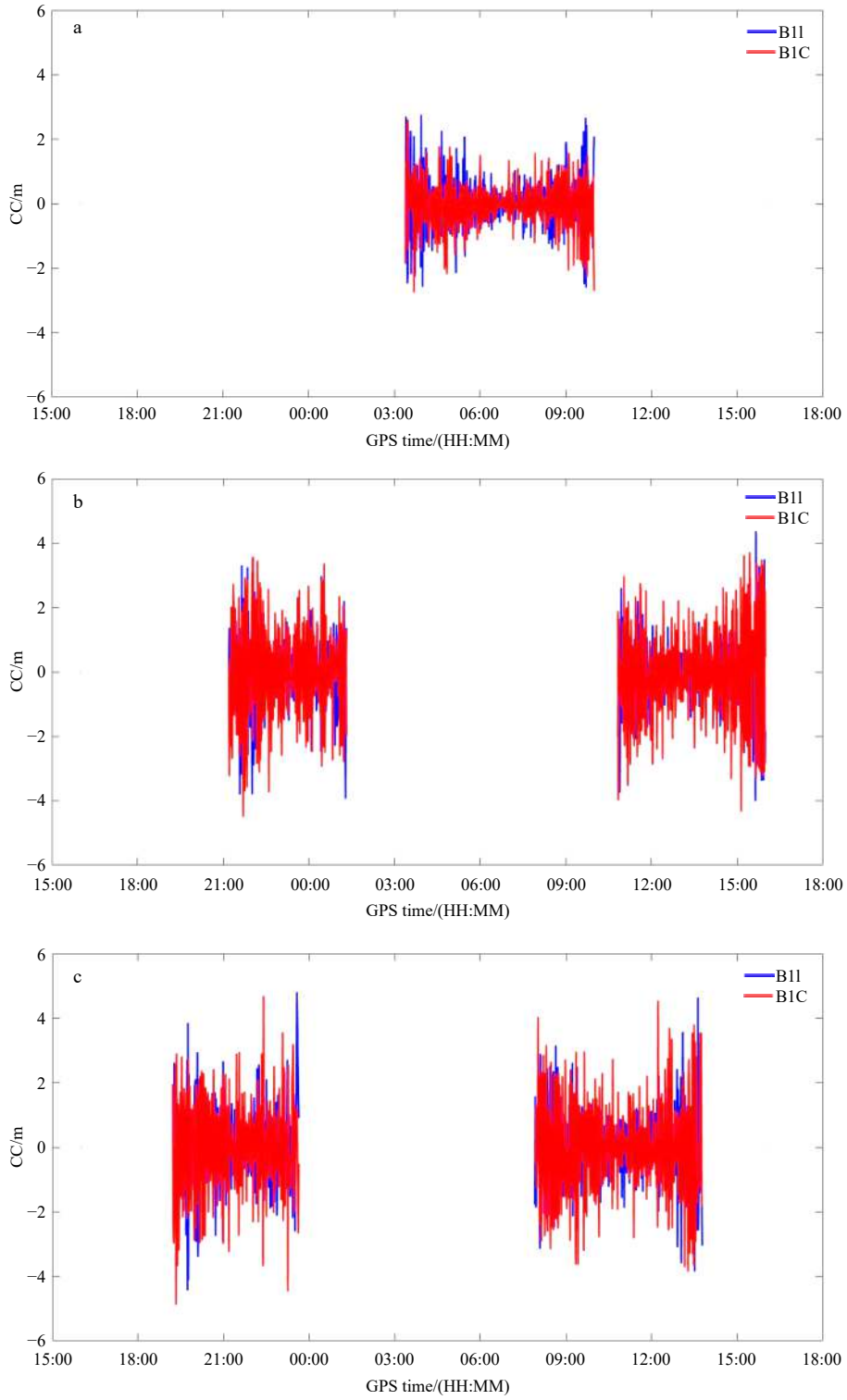

Fig. 11. Code-minus-carrier combination (CC) of latitude around 45° (DOY 204) (a), CC of latitude around 60° (DOY 209) (b), and CC of latitude around 75° (DOY 215) (c).

sea area and the Arctic Ocean. As the elevation angle increases, the SNR value tends to increase slowly, while the MP value tends to decrease slowly.

(3) As the latitude increases, the value of DOP shows a large variation. Taking the value of GDOP as an example, most of the values are below 3 in the 45° latitudes and 60° latitudes ocean. However, the value of GDOP is much larger in 70° latitudes ocean and the maximum is even more than 7. The value of DOP is related to the distribution of BDS satellites closely. These results indicate that the BeiDou satellite geometry distribution in the high latitudes is not as good as in the mid-latitude area. With the construction of BDS, BDS will provide a better service on a global scale in the future.

(4) The CC values of B1I and BIC frequencies range from –5 m

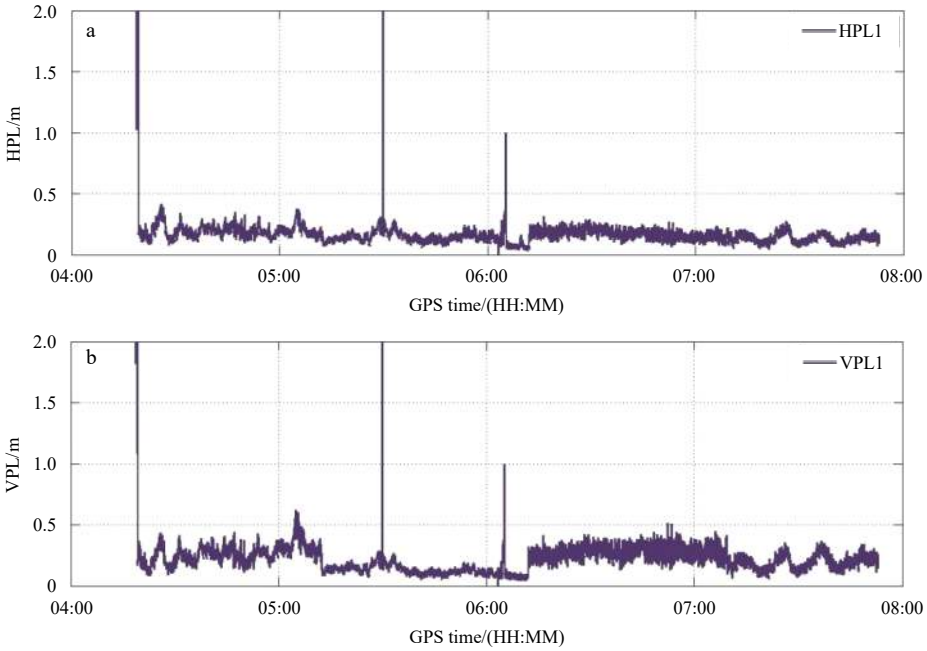

Fig. 12. Horizontal improved isotropy-based protection level of BDS3 data received at mid-high latitudes (DOY 217) (a), and vertical improved isotropy-based protection level of BDS3 data received at mid-high latitudes (DOY 217) (b).

to 5 m in the mid-latitude sea area and the Arctic Ocean, which means the pseudorange noise is small.

(5) In order to evaluate the PPP performance of BDS in the Arctic Ocean, this paper proposes an improved isotropy-based protection level based on RAIM theory. The proposed method uses median filter to smooth the gross error. First, the effectiveness of the improved algorithm was verified by using data from the IGS Station Tixi. Then, the accuracy of BDS PPP in the Arctic Ocean was calculated by using this algorithm. The results show that the improved protection level can reflect the fluctuation of gross error and the level of position bias very well. The kinematic positioning accuracy can reach the decimeter level in the horizontal and vertical directions, which meets the precision requirements of maritime navigation.

Acknowledgements

Thanks to China's 9th Arctic Science Expedition for its support of data collection in this paper.

References

Abdel-Salam M. 2005. Precise point positioning using un-differenced code and carrier phase observations [dissertation]. Calgary, Canada: University of Calgary

Cai Changsheng, He Chang, Santerre R, et al. 2016. A comparative analysis of measurement noise and multipath for four constellations: GPS, BeiDou, GLONASS and Galileo. Survey Review, 48(349): 287–295, doi: 10.1179/1752270615Y.0000000032

CSNO. 2019. BeiDou Navigation Satellite System Signal in Space Interface Control Document Open Service Signal B1I A (Version 3.0). Beijing: China Satellite Navigation Office

Du Yujun, Wang Zemin, An Jiachun, et al. 2015. Positioning analysis of BeiDou navigation satellite system over ocean and Antarctic regions. Chinese Journal of Polar Research, 27(1): 91–97

Feng Shaojun, Ochieng W, Moore T, et al. 2009. Carrier phase-based integrity monitoring for high-accuracy positioning. GPS Solutions, 13(1): 13–22, doi: 10.1007/s10291-008-0093-0

Gao Yang, Shen Xiaobing. 2002. A new method for carrier-phase-based precise point positioning. Navigation, 49(2): 109–116, doi: 10.1002/j.2161-4296.2002.tb00260.x

Geng Jianghui, Teferle F N, Shi Chuang, et al. 2009. Ambiguity resolution in precise point positioning with hourly data. GPS Solutions, 13(4): 263–270, doi: 10.1007/s10291-009-0119-2

Gumilar I, Bramanto B, Kuntjoro W, et al. 2018. Contribution of BeiDou satellite system for long baseline GNSS measurement in Indonesia. IOP Conference Series: Earth and Environmental Science, 149(1): 012070, doi: 10.1088/1755-1315/149/1/012070

Guo Fei. 2013. Theory and methodology of quality control and quality analysis for GPS precise point positioning [dissertation] . Wuhan: Wuhan University

Hauschild A, Montenbruck O, Sleewaegen J, et al. 2012. Characterization of compass M-1 signals. GPS Solutions, 16(1): 117–126, doi: 10.1007/s10291-011-0210-3

Lee Y C. 1986. Analysis of range and position comparison methods as a means to provide GPS integrity in the user receiver. In: Proceedings of the 42nd Annual Meeting-Institute of Navigation. Washington, DC, USA: Institute of Navigation, 1–4

Lee Y C. 2006. A new improved RAIM method based on the optimally weighted average solution (OWAS) under the assumption of a single fault. In: Proceedings of the ION NTM. Monterey, CA, USA: ION

Li Min, Qu Lizhong, Zhao Qile, et al. 2014. Precise point positioning with the BeiDou navigation satellite system. Sensors, 14(1): 927–943, doi: 10.3390/s140100927

Liu Zenghong, Wu Xiaofen, Xu Jianping, et al. 2017. China Argo project: progress in China Argo ocean observations and data applications. Acta Oceanologica Sinica, 36(6): 1–11, doi: 10.1007/s13131-017-1035-x

Lou Yidong, Li Xianjie, Zheng Fu, et al. 2018. Assessment and impact on BDS positioning performance analysis of recent BDS IGSO-6 satellite. Journal of Navigation, 71(3): 729–748, doi: 10.1017/s0373463317000832

Lu Chengliang, Zhang Shengkai, E Dongchen. 2011. Analysis of GPS data in Antarctic. Journal of Geodesy and Geodynamic, 31(2): 117–120

Luo Xiaowen, Zhang Tao, Gao Jinyao, et al. 2015. Estimation of annual variation of water vapor in the Arctic Ocean between 80°–87°N using shipborne GPS data based on kinematic precise point positioning. Acta Oceanologica Sinica, 34(6): 1–4, doi: 10.1007/s13131-015-0680-1

Luo Xiaomin, Gu Shengfeng, Lou Yidong, et al. 2018. Assessing the performance of GPS precise point positioning under different

geomagnetic storm conditions during solar cycle 24. Sensors, 18(6): 1784, doi: 10.3390/s18061784

Madrid P F N, Saenz M A, Varo C M, et al. 2015a. Computing meaningful integrity bounds of a low-cost Kalman-filtered navigation solution in urban environments. In: Proceedings of the 28th International Technical Meeting of the Satellite Division of the Institute of Navigation (ION GNSS+2015). Tampa, FL, USA: ION, 2914–2925

Madrid P F N, Saenz M A, Varo C M, et al. 2015b. New approach for integrity bounds computation applied to advanced precise positioning applications. In: Proceedings of the 28th International Technical Meeting of the Satellite Division of the Institute of Navigation. (ION GNSS+2015). Tampa, FL, USA: ION, 2821–2834

Merino M M R, Lainez M D. 2012. Integrity for advanced precise positioning applications. Transactions of the Japan Society of Mechanical Engineers C, 58(551): 2249–2254, doi: 10.1299/kikaic.58.2249

Miguel A S, Joaquin C S M. 2009. An error isotropy-based approach for multiple fault conditions. Inside CNSS, 2009,1: 28–36

Montenbruck O, Hauschild A, Steigenberger P, et al. 2013. Initial assessment of the COMPASS/BeiDou-2 regional navigation satellite system. GPS Solutions, 17(2): 211–222, doi: 10.1007/s10291-012-0272-x

Tu Rui, Zhang Pengfei, Zhang Rui, et al. 2018. Modeling and assessment of precise time transfer by using BeiDou navigation satellite system triple-frequency signals. Sensors, 18(4): 1017, doi: 10.3390/s18041017

Wang Guangxing, De Jong K, Zhao Qile, et al. 2015. Multipath analysis of code measurements for BeiDou geostationary satellites. GPS Solutions, 19(1): 129–139, doi: 10.1007/s10291-014-0374-8

Wang Ershen, Jia Chaoying, Tong Gang, et al. 2018. Fault detection and isolation in GPS receiver autonomous integrity monitoring based on chaos particle swarm optimization-particle filter algorithm. Advances in Space Research, 61(5): 1260–1272, doi: 10.1016/j.asr.2017.12.016

Wang Minghua, Wang Jiexian, Dong Danan, et al. 2019. Performance of BDS-3: satellite visibility and dilution of precision. GPS Solutions, 23(2): 56, doi: 10.1007/s10291-019-0847-x

Wanninger L, Beer S. 2015. BeiDou satellite-induced code Pseudorange variations: diagnosis and therapy. GPS Solutions, 19(4): 639–648, doi: 10.1007/s10291-014-0423-3

Xiao Wei, Liu Wenxiang, Sun Guangfu. 2016. Modernization milestone: BeiDou M2-S initial signal analysis. GPS Solutions, 20(1): 125–133, doi: 10.1007/s10291-015-0496-7

Xiao Guorui, Sui lifen, Herk B, et al. 2018. Estimating satellite phase fractional cycle biases based on Kalman filter. GPS Solutions, 22(3): 82, doi: 10.1007/s10291-018-0749-3

Xu Aigong, Xu Zongqiu, Ge Maorong, et al. 2013. Estimating zenith tropospheric delays from BeiDou navigation satellite system observations. Sensors, 13(4): 4514–4526, doi: 10.3390/s130404514

Xu Yangyin, Yang Yuanxi, He Haibo, et al. 2018. Quality analysis of the range measurement signals of test satellites in BeiDou global system. Geomatics and Information Science of Wuhan University (in Chinese), 43(8): 1214–1221

Yan Xincun, Ouyang Yongzhong, Sun Fuping. 2012. Reliability evaluation method of precise point positioning algorithm results. GNSS World of China, 37(6): 9–12,16

Yang Yuanxi. 2010. Progress, contribution and challenges of Compass/BeiDou satellite navigation system. Acta Geodaetica et Cartographica Sinica, 39(1): 1–6

Yang Yuanxi, Li Jinlong, Wang Aibing, et al. 2014. Preliminary assessment of the navigation and positioning performance of BeiDou regional navigation satellite system. Science China: Earth Sciences, 57(1): 144–152, doi: 10.1007/s11430-013-4769-0

Yang Yuanxi, Xu Junyi. 2016. Navigation performance of BeiDou in Polar Area. Geomatics and Information Science of Wuhan University (in Chinese), 41(1): 15–20

Yang Yuanxi, Xu Yangyin, Li Jinlong, et al. 2018. Progress and performance evaluation of BeiDou global navigation satellite system: Data analysis based on BDS-3 demonstration system. Science China: Earth Sciences, 61(5): 614–624, doi: 10.1007/s11430-017-9186-9

Zhao Qile, Wang Chen, Guo Jing, et al. 2015. Assessment of the contribution of BeiDou GEO, IGSO, and MEO satellites to PPP in Asia-Pacific region. Sensors, 15(12): 29970–29983, doi: 10.3390/s151229780

Zumberge J F, Heflin M B, Jefferson D C, et al. 1997. Precise point positioning for the efficient and robust analysis of GPS data from large networks. Journal of Geophysical Research: Solid Earth, 102(B3): 5005–5017, doi: 10.1029/96jb03860